RESEARCH ARTICLE

WILEY **Journal of RAMAN SPECTROSCOPY**

Lattice dynamics study of cubic Tb$_2$O$_3$

Jordi Ibáñez[1] | Oriol Blázquez[2] | Sergi Hernández[2] | Blas Garrido[2] |

Plácida Rodríguez-Hernández[3] | Alfonso Muñoz[3] | Matias Velázquez[4] |

Philippe Veber[4,5] | Francisco Javier Manjón[6]

[1] Institute of Earth Sciences Jaume Almera (CSIC), Barcelona, Spain

[2] MIND-IN$_2$UB, Departament d'Electrònica, Universitat de Barcelona, Barcelona, Spain

[3] Departamento de Física, Instituto de Materiales y Nanotecnología, MALTA Consolider Team, Universidad de La Laguna, San Cristóbal de la Laguna, Spain

[4] CNRS, Université de Bordeaux, Pessac cedex, France

[5] CNRS, Institut Lumière Matière, Université Lyon, Université Claude Bernard Lyon 1, UMR 5306, Villeurbanne, France

[6] Instituto de Diseño para la Fabricación y Producción Automatizada, MALTA Consolider Team, Universitat Politècnica de València, València, Spain

Correspondence

Jordi Ibáñez, Institute of Earth Sciences Jaume Almera (CSIC), Lluís Solé i Sabarís s/n, 08028 Barcelona, Catalonia, Spain.
Email: jibanez@ictja.csic.es

Francisco Javier Manjón, Instituto de Diseño para la Fabricación y Producción Automatizada, MALTA Consolider Team, Universitat Politècnica de València, València 46022, Spain.
Email: fjmanjon@fis.upv.es

Funding information

Spanish Ministerio de Economía y Competitividad, Grant/Award Numbers: FIS2017-2017-83295-P, MAT2016-75586-C4-2-P/3-P, MAT2015-71035-R and MAT2015-71070-REDC

Abstract

We report a joint experimental and theoretical study of the lattice dynamics of cubic Tb$_2$O$_3$. Up to 16 optical Raman-active modes have been observed with polarized and unpolarized Raman scattering measurements on a high-quality Tb$_2$O$_3$ single crystal. The measured wavenumbers have been compared with those of other rare-earth (RE) and related sesquioxides with cubic (C-type or bixbyite) structure. First-principles calculations have allowed us to assign the symmetry of the experimentally observed Raman-active modes. Additional lattice-dynamical calculations on the related cubic RE sesquioxides Dy$_2$O$_3$, Gd$_2$O$_3$, Eu$_2$O$_3$, and Sm$_2$O$_3$ indicate that the phonon wavenumbers of the Raman-active modes in these compounds are monotonically reduced with increasing the lattice parameter along the Dy$_2$O$_3$-Tb$_2$O$_3$-Gd$_2$O$_3$-Eu$_2$O$_3$-Sm$_2$O$_3$ series, thus prompting for a revision of the experimental Raman spectra of some of these compounds (mainly Eu$_2$O$_3$ but also Gd$_2$O$_3$).

KEYWORDS

lattice dynamics ab initio calculations, Raman scattering, rare-earth sesquioxides, Tb$_2$O$_3$, Terbium oxide

1 | INTRODUCTION

Rare-earth (RE) sesquioxides (R$_2$O$_3$, R = Y, Sc, or lanthanide) are interesting materials due to their remarkable fundamental properties and potential applications. These compounds may enable a wide range of technological advances including light emitters, catalysts, or high-dielectric constant (high-k) gates. Among this family of compounds, terbium oxide (Tb$_2$O$_3$) has attracted considerable attention in the last few years as a high-k material[1–3] and

also as an active material for high-performance optoelectronic devices.[4–6] Recently, it has been shown that millimeter-sized C-type Tb_2O_3 pure single crystals can be grown with a controlled atmosphere flux method, using melting temperatures much lower than those of pure Tb_2O_3.[7] The high-quality cubic Tb_2O_3 crystals thus obtained are highly promising for applications in optics and photonics.

It is well-known that, depending on the RE ionic radius and temperature, R_2O_3 compounds may exhibit different polymorphic modifications. These may be cubic (C-type phase), monoclinic (B-type phase), or hexagonal (A-type phase). The C-type or bixbyite structure (space group $Ia\overline{3}$, No. 206, Z = 16) is usually the stable phase at room temperature in the case of the heavier lanthanides, such as Tb_2O_3, and also in related sesquioxides, such as Mn_2O_3, In_2O_3, and Tl_2O_3. In addition, different stoichiometries can be grown due to different oxidation states of the RE cation. This is particularly relevant for the binary Tb oxides, where Tb^{3+} and Tb^{4+} states coexist and therefore different TbO_x compounds with $1.5 < x < 2$ are usually formed. Thus, it is highly important to properly characterize the as-grown RE oxide samples in order to identify the coexisting phases and stoichiometries.

Raman scattering (RS) spectroscopy is a powerful nondestructive analytical tool that provides useful information, among others, about the crystal quality, structural properties, and lattice dynamics of solid-state materials. Many different studies have been devoted to investigate the RS properties of C-type RE sesquioxides (see Ref.[8] and references therein) or their solid solutions.[9] It is now clear that the high-wavenumber Raman peaks of C-type R_2O_3 compounds, involving mainly O vibrations, basically display a monotonic behavior as a function of the lattice parameter. In turn, the wavenumber of the low-wavenumber modes involving lanthanide vibrations is almost constant for the whole family of R_2O_3 compounds, except Sc_2O_3 and Y_2O_3 due to the much smaller mass of the R ion.[8] However, there are still open questions in relation to the vibrational properties of some of these compounds. For instance, cubic Eu_2O_3 seems to exhibit an anomalous behavior (softening). The anomaly has been ascribed to either the presence of oxygen vacancies or to the specific electronic structure of Eu^{3+} relative to the rest of lanthanides.[8] In spite of the large number of papers devoted to the RS properties of R_2O_3 compounds, the information about Tb_2O_3 is still scarce.[10]

The aim of the present work is to investigate the lattice-dynamical properties of Tb_2O_3. For this purpose, we have performed RS measurements on a high-quality Tb_2O_3 single crystal. Polarized Raman spectra, in combination with first-principles density functional theory (DFT) calculations of the zone-center phonons, have allowed us to unambiguously identify the first-order Raman peaks of Tb_2O_3. The

DFT calculations are extended to other R_2O_3 compounds (R = Sm, Eu, Gd, Dy), which allows us to shed additional light on the possible anomalous behavior observed in Eu_2O_3.

2 | EXPERIMENTAL METHODS

Cubic Tb_2O_3 single crystals were grown by a controlled atmosphere flux method using a $Li_6Tb(BO_3)_3$ solvent and a Tb_2O_3 solute. The flux solution was melted at 1,230°C (less than half the melting temperature of Tb_2O_3) and subsequently cooled down slowly to 1,160°C. After cutting and polishing, almost inclusion-free, millimeter-sized crystals oriented along the [112] crystallographic orientation were obtained. The growth was unseeded, so it was fortuitous that we obtained the [112] orientation, which was determined by the Laue method on a Delta Technologies International GM WS Series X-Ray goniometer head. Powder X-ray diffraction experiments were performed within the $8° \leq 2\theta \leq 80°$ range on carefully ground and sieved crystals by using a PANalytical X'Pert Pro MPD diffractometer (Cu Kα1 Kα2 radiation). Le Bail fits confirmed the cubic $Ia\overline{3}$ symmetry and allowed extracting a lattice parameter $a = 10.7323(3)$ Å. No reflections arising from $Li_6Tb(BO_3)_3$ or from other phases were detected in the X-ray diffraction (XRD) scans. Details of the growth method and the structural properties of the Tb_2O_3 crystals can be found in Ref.[7]

Room-temperature polarized and unpolarized micro-RS measurements were excited with the 532-nm line of a solid state laser. Inelastically scattered light was collected with a Horiba Jobin Yvon LabRAM HR spectrometer equipped with an edge filter that cuts Raman signals below ~50 cm^{-1} and a thermoelectrically cooled multi-channel Charge Coupled Device (CCD) detector enabling a spectral resolution better than 2 cm^{-1}. Unpolarized RS measurements were also performed at 80 K by using a Linkam microscope stage. Different Raman spectra were acquired at various sample orientations, relative to the polarization of the incoming light, by rotating the sample around the [112] direction (i.e., the crystal orientation). These measurements allowed us to properly identify all the features that appear in the Raman spectra of Tb_2O_3.

3 | FIRST-PRINCIPLES CALCULATIONS

Ab initio total-energy calculations at 0 GPa and 0 K were performed within the framework of DFT for several C-type RE sesquioxides: Tb_2O_3, Dy_2O_3, Gd_2O_3, Eu_2O_3, and Sm_2O_3.[11] In the cubic structure, O atoms are located at 48e Wyckoff sites and RE atoms at 8b and 24d sites.

The Vienna ab initio Simulation Package[12] was used to perform calculations with the pseudopotential method and the projector augmented waves scheme.[13,14] The exchange-correlation energy was obtained in the generalized gradient approximation using the Perdew-Burke-Enzerhof (PBE) prescription[15] and its extension to the solid state, PBEsol.[16] A dense $6 \times 6 \times 6$ Monkhorst $-$Pack[17] grid of special k-points and a plane-wave basis set with energy cutoffs of 530 eV were used.

Table S1 shows the resulting zero-pressure lattice parameter (a_0), bulk modulus (B_0), and first-derivative of the bulk modulus (B') calculated for Tb_2O_3, both with PBE and PBEsol functionals, after full structural optimization of the cubic crystal lattice at a set of chosen pressures. The corresponding B_0 and B' values were obtained with a fit to the P-V data resulting from the structural optimizations at different pressures, using a third-order Birch–Murnaghan equation of state. In the relaxed optimized configurations, the resulting forces on the atoms are less than 0.004 eV/Å, with deviations of the stress tensor from the hydrostatic form (diagonal tensor) lower than 0.1 GPa. As can be seen in Table S1, the zero-pressure lattice parameter calculated with both PBE and PBEsol differs by less than ~1% with respect to the experimental data. However, the PBE value is much closer to the experimental value. Owing to this, the larger lattice spacing obtained with PBE gives rise to a sizably larger compressibility relative to PBEsol (see Table S1). Although the theoretical PBE lattice parameter is in better agreement with the experimental value, in the present work, we rely on the PBEsol functional because, as will be shown below (and as also found in other related compounds such as C-type In_2O_3),[18] it provides much better results for the present lattice-dynamical calculations.

The elastic constants of C-type Tb_2O_3 were also calculated within DFT-PBEsol as implemented in Vienna ab initio Simulation Package. Details of ab initio calculations of the mechanical properties of similar sesquioxide compounds can be found elsewhere.[19] The following values were obtained for the three independent elastic constants of the cubic lattice of Tb_2O_3: C_{11} = 221.62 GPa, C_{12} = 116.52 GPa, and C_{44} = 72.67 GPa. With these data, the zero-pressure bulk modulus can be independently obtained using the expression $B_0 = (C_{11} + 2C_{12})/3$ for materials with cubic symmetry. This formula gives a value of 151.5 GPa for Tb_2O_3, which is in very good agreement with the value obtained after the structural relaxation (B_0 = 151.24 GPa, see Table S1), showing the consistency of the present calculations.

Lattice-dynamics calculations were also performed for Dy_2O_3, Tb_2O_3, Gd_2O_3, Eu_2O_3, and Sm_2O_3. Phonon wavenumbers for all these compounds were calculated at the Γ point using the direct-force constant approach,[20]

with the PBEsol functional to compute the atomic forces. For comparison purposes, the zone-center (Γ point) phonon wavenumbers of Tb_2O_3 were also obtained with the PBE functional. For this compound, calculations (with the PBEsol functional) of the phonon dispersion and one-phonon density of states were also carried out along high-symmetry directions of the Brillouin zone, using a $2 \times 2 \times 2$ supercell. Figure 1 shows the Tb- and O-projected phonon density of states for cubic Tb_2O_3. Our calculations show that the optical phonons of Tb_2O_3 involving O (Tb) atoms have wavenumbers higher (lower) than 250 cm^{-1} (225 cm^{-1}), leaving a small gap around 25 cm^{-1} between both types of modes. The resulting gap is significantly larger in the case of the zone-center optical phonons (see bottom of Figure 2), because the wavenumber of the Raman-active phonons of Tb_2O_3 involving Tb (O) vibrations is below (above) 200 cm^{-1} (300 cm^{-1}), that is, leaving a gap larger than 100 cm^{-1}.

4 | RESULTS AND DISCUSSION

As discussed in different previous works of C-type RE and bixbyite-type sesquioxides,[8,21,22] the primitive cell of C-type Tb_2O_3 contains eight formula units. Therefore, group theory predicts that this structure should have 120 zone-center vibrational modes: $\Gamma = 4A_g$ (R) $+ 4E_g$ (R) $+ 14F_g$ (R) $+ 5A_u + 5E_u + 17F_u$ (infrared), where E and F (that it is also noted T in some literature) modes are double and triple degenerated, respectively. The 22 gerade (g) modes are Raman-active (R) modes, the 16 F_u modes are infrared-active modes, the A_u and E_u are silent modes,
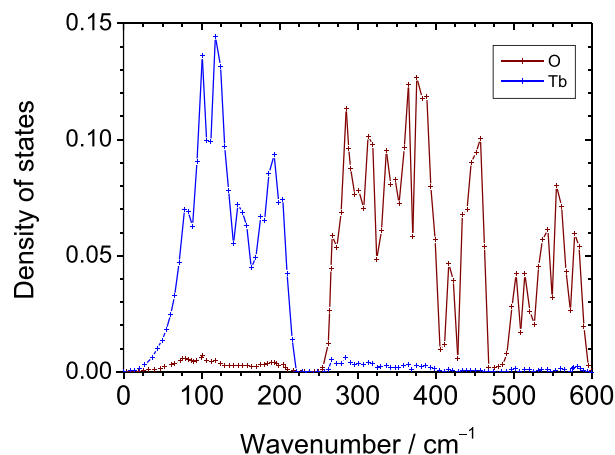

FIGURE 1 Tb- and O-projected PDOS of Tb_2O_3 as obtained with first-principles DFT-GGA calculations using the PBEsol functional. DFT: density functional theory; GGA: generalized gradient approximation; PDOS: phonon density of states [Colour figure can be viewed at wileyonlinelibrary.com]
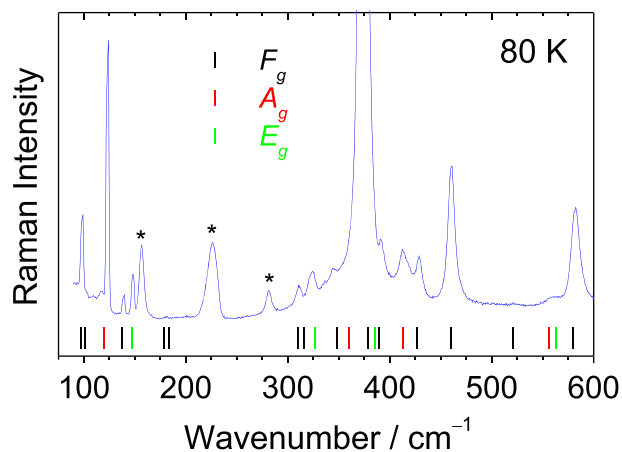
FIGURE 2 Unpolarized Raman spectrum of Tb_2O_3 acquired at 80 K. Peaks marked with an asterisk can be tentatively assigned to local vibrational modes. In the bottom of the figure, the position of the vertical lines indicates the wavenumber of the Raman-active phonons of Tb_2O_3 (F_g, A_g and E_g symmetries) as obtained with first-principles DFT-GGA calculations using the PBEsol functional. DFT: density functional theory; GGA: generalized gradient approximation [Colour figure can be viewed at wileyonlinelibrary.com]

and one F_u mode corresponds to the acoustic vibrations. Figure 2 shows an unpolarized Raman spectrum of Tb_2O_3 obtained at 80 K together with the theoretical wavenumbers of the 22 Raman-active modes as obtained with the PBEsol functional. Up to 16 different modes show up in the low-temperature spectrum (bands marked with an asterisk probably correspond to local vibrational modes, see below). This large number of measured modes is higher than that reported for most of the C-type sesquioxides.[8] However, it is similar to the number of Raman-active modes recently obtained in related bixbyite compounds such as In_2O_3.[18,23]

A comparison between the calculated and experimental wavenumbers of the Raman-active optical phonons of Tb_2O_3 can be found in Table 1. Band assignments will be later confirmed in terms of additional RS measurements with different scattering geometries. As can be seen in Figure 2 and in Table 1, excellent agreement is found between the experimental wavenumbers of most Raman peaks and the calculated values for the Raman-active modes when the PBEsol functional is used. In contrast, the results obtained with the PBE functional (see Table 1) tend to underestimate the wavenumber of most optical phonon modes, especially those involving O vibrations. In general, PBEsol calculations in sesquioxide compounds are found to correctly predict their structural and vibrational properties. They only slightly underestimate the wavenumbers observed at room conditions, as is the case of Tb_2O_3 in the present work or, for instance, the case of cubic In_2O_3.[18]

TABLE 1 Experimental (80 and 300 K) and theoretical (0 K) wavenumbers of the Raman-active phonons of cubic Tb_2O_3

Symmetry	ω_{theory} / cm^{-1}		$\omega_{exp.}$ / cm^{-1}	
	PBE	**PBESOL**	**80 K**	**300 K**
F_g^1	95.05	96.69	98.1(2)	94.5(5)
F_g^2	98.36	101.05		
A_g^1	114.29	119.33	123.4(2)	118.2(5)
F_g^3	132.35	137.31	139.0(2)	134.2(5)
E_g^1	143.13	147.16	148.1(2)	144.3(5)
F_g^4	171.36	178.15		
F_g^5	177.48	183.63	181(1)	
F_g^6	295.32	310.35	310.9(5)	305(1)
F_g^7	300.68	315.36		
E_g^2	311.07	326.86	324.1(5)	320.8(5)
F_g^8	330.57	348.42	345.3(5)	
A_g^2	345.04	359.55		
F_g^9	360.67	379.03	374.3(2)	366.9(5)
E_g^3	365.13	384.99		
F_g^{10}	372.74	388.90	391.5(5)	
A_g^3	396.77	412.95	413.3(5)	408.2(5)
F_g^{11}	411.15	426.37	428.9(5)	421(1)
F_g^{12}	442.06	459.65	460.4(2)	453(1)
F_g^{13}	505.15	520.73	521.5(5)	
A_g^4	541.45	556.49	559(1)	
E_g^4	548.42	563.14		
F_g^{14}	563.49	579.46	582.4(5)	577(1)

Note. Theoretical wavenumbers obtained with DFT-GGA calculations using a PBE and a PBEsol functional are given for comparison. DFT: density functional theory; GGA: generalized gradient approximation.

As in the rest of C-type R_2O_3 sesquioxides,[8] the Raman spectrum of Tb_2O_3 is dominated by a strong peak corresponding to a F_g mode. This peak is located at ~370 cm^{-1} in the case of Tb_2O_3. In contrast, some of the Raman-active modes are barely visible or, simply, do not show up in the Raman spectrum. It must be noted that the bands marked with an asterisk in Figure 2 cannot be ascribed to first-order RS by lattice phonons, because no optical phonon modes are expected in this spectral region. Similarly, XRD measurements indicate that this sample does not contain other Tb oxide phases that could be responsible for these peaks. Taking into account the relatively high intensity of these bands relative to those of bulk Tb_2O_3, the XRD results suggest that they cannot arise from microdomains of noncubic Tb_2O_3 phases or other Tb oxides. On the other hand, they can neither be assigned to second-order Raman modes owing to their temperature behavior. Indeed, RS measurements acquired at different temperatures (not shown)

revealed that the intensity of these features decreases with increasing temperature, which is opposite to the expected behavior for second-order modes. These bands cannot either be assigned to photoluminescence peaks arising from $^5D_4$ to $^7F_5$ intra-4f electronic radiative transitions in Tb^{3+} ions,[24] because they also show up in Raman spectra excited with longer wavelengths (λ = 785 nm, spectra not shown). More work is required in order to ascertain whether these features can be ascribed, for instance, to local vibrational modes.

On the other hand, the single-crystal sample studied in this work allowed us to carry out polarized RS measurements. Such measurements, in combination with the results of the DFT calculations, are helpful to confirm the assignments of the different peaks that show up in the unpolarized Raman spectra. Figure 3 shows two different room-temperature Raman spectra of Tb_2O_3 obtained in parallel and perpendicular polarization configurations, respectively. Note that these room-temperature spectra do not allow us to detect the weakest features around the peak at ~370 cm^{-1} that were detected at 80 K. In any case, the A_g and E_g modes can be easily identified in Figure 3 because they become extinct under perpendicular polarization. In A_g modes, this behavior is expected because the Raman tensor of this mode is just proportional to the identity matrix. This is the case, for instance, of the sharp peak at ~120 cm^{-1} that corresponds to an A_g mode in most R_2O_3 sesquioxides.[8] On the other hand, in E_g modes, the observed intensity drop is a consequence of the particular (unknown) orientation of the sample used to perform the polarized RS measurements. This behavior is displayed, for instance, by the peak at ~148 cm^{-1}, which can be unambiguously attributed to an E_g optical mode thanks to our DFT results. In contrast, the intensity

of F_g modes is barely changed with polarization, as is the case of several of the low-wavenumber modes that are visible in Figures 2 and 3.

The room-temperature polarized Raman spectra of Figure 3 also allow one to correctly locate the weak F_g peaks that appear at ~310 and ~420 cm^{-1}, in good agreement with the DFT calculations using the PBEsol functional. On the other hand, these spectra indicate that the weak feature at ~410 cm^{-1} corresponds to an A_g mode, as also predicted by DFT calculations (see Figure 2 and Table 1). This value is somewhat lower than that expected taking into account the values for the high-wavenumber A_g mode reported in Ref.[8] for the C-type R_2O_3 compounds (for instance, 425 cm^{-1} in Dy_2O_3 and 414 cm^{-1} in Gd_2O_3). This difference could be due to the fact that this mode was wrongly assigned in some of the previous studies, especially in Gd_2O_3. On the other hand, the spectra of Figure 3 seem to indicate that the peak at ~325 cm^{-1} has mainly contribution from an E_g mode, because the intensity of this peak almost vanishes under perpendicular polarization. In this context, we would like to note that the mode corresponding to this spectral region in other R_2O_3 compounds has been previously attributed to $F_g + E_g$ symmetry. The reason is the possible proximity between one F_g mode and one E_g mode in most R_2O_3 compounds.[8] The present results (experimental and ab initio), at least in the case of Tb_2O_3, suggest that this peak has mainly E_g symmetry. And, clearly, the Raman shift of this mode is consistent with the values reported in other R_2O_3 compounds in this wavenumber region.[8]

As anticipated, the phonon wavenumbers measured in this work are consistent with the trends exhibited by C-type R_2O_3 sesquioxides as a function of the unit cell parameter or, equivalently, as a function of the R–O cation-anion distance. The high-wavenumber phonons involving O vibrations show a clear monotonic upward shift with decreasing the lattice parameter.[8] This result can be attributed to the fact that the effective spring constant associated with the different R–O bonds is enhanced when the interatomic distances are reduced.[25] This, in turn, is a consequence of the reduction of the ionic radius with increasing the number of f-electrons in the shell of the R cation. In contrast, the low-wavenumber phonons (i.e., those involving oscillations of the R cation, as seen in Figure 1 for the case of Tb_2O_3) barely depend on R because the upward wavenumber shift due to the stiffening of the spring constant is counteracted by the increase of the atomic mass of R, except in the case of Y_2O_3 and Sc_2O_3.[8]

We would like to remark that several works have pointed out that the phonon wavenumbers of Eu_2O_3 exhibit a somewhat distinct behavior in comparison with other RE sesquioxides.[8,10] In particular, the high-wavenumber Raman peaks of Eu_2O_3 have been observed to
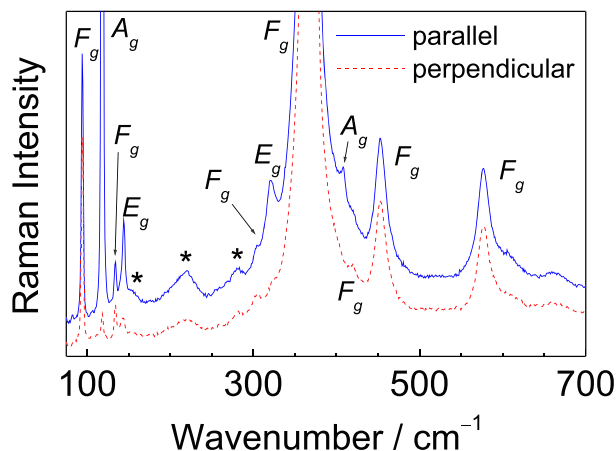

FIGURE 3 Polarized Raman spectra of Tb_2O_3 acquired at room temperature with parallel and perpendicular polarization configurations. Peaks marked with an asterisk can be tentatively assigned to local vibrational modes [Colour figure can be viewed at wileyonlinelibrary.com]

appear at wavenumbers that are sizably lower than those measured on Gd_2O_3 and Sm_2O_3,[8] that is, its neighboring compounds in terms of atomic number of R and lattice parameter. This observation could be related to the specific electronic configuration of Eu^{3+} relative to the rest of lanthanides[10] but also to the presence of O vacancies in the crystal lattice of Eu_2O_3.[8] In order to compare the lattice-dynamical properties of Tb_2O_3 with those of closely related R_2O_3 compounds and also to shed light on the anomalous behavior of Eu_2O_3, we have performed additional first-principles lattice-dynamical calculations of the Raman-active modes in Eu_2O_3, Sm_2O_3, Gd_2O_3, and Dy_2O_3. Calculations have been performed using PBEsol functionals (see Table S2). The results, plotted in Figure 4, show that the high-wavenumber (>300 cm^{-1}) Raman-active modes of all these five compounds display a monotonic wavenumber decrease as a function of the lattice parameter, that is, as a function of the ionic size of the cation. These data are in agreement with the general trend exhibited by all the R_2O_3 compounds.[8] Thus, no softening of the high-wavenumber Raman modes is predicted by the present DFT-generalized gradient approximation calculations for Eu_2O_3. On the other hand, our calculations also show that the wavenumber of the A_g Raman mode of Tb_2O_3, around 400 cm^{-1} must be larger than that of Gd_2O_3, thus prompting for a revision of the anomalous value reported in Ref.[8] for Gd_2O_3.

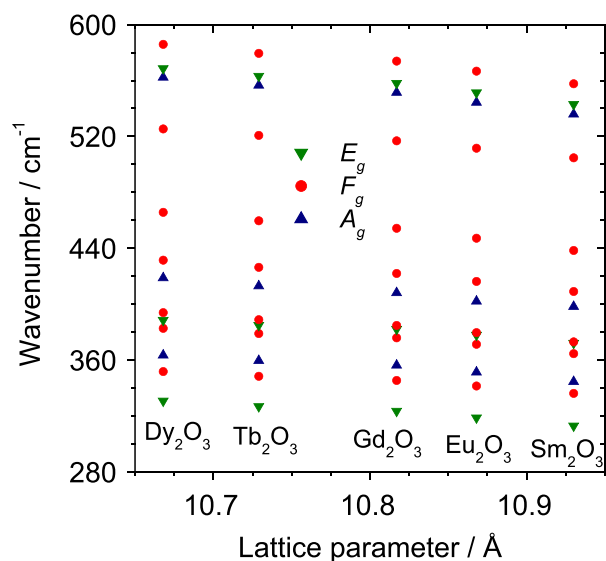Some authors have attributed the wavenumber reduction of the high-wavenumber optical modes of Eu_2O_3 and

FIGURE 4 Theoretical wavenumber values of the high-wavenumber Raman-active phonons of R_2O_3 compounds (R = Dy, Tb, Gd, Eu, Sm) as a function of the lattice parameter, as obtained with first-principles DFT-GGA calculations using PBEsol functionals. DFT: density functional theory; GGA: generalized gradient approximation [Colour figure can be viewed at wileyonlinelibrary.com]

Yb_2O_3 to the larger deformation of the electron shells of Eu and Yb ions than those of other lanthanides. This has been associated to the presence of shallow f-states[10]; however, it is clear that such effect cannot be linked to the half-filled $4f^7$ configuration of the 2+ oxidation state, which is more stable than the $4f^6$ configuration of Eu^{3+}, because Eu ion has a 3+ oxidation state in Eu_2O_3. Interestingly, the low-wavenumber modes of Eu_2O_3, that is, those actually involving Eu vibrations, do not display any sizable wavenumber change relative to the rest of R_2O_3 compounds.[8] This observation, together with the results of the DFT calculations (Figure 4), suggests that the anomalous behavior of the high-wavenumber Raman modes of Eu_2O_3 is not related to its specific electronic configuration. Thus, the presence of O vacancies in the crystal structure of Eu_2O_3 could be responsible for the wavenumber reduction exhibited by some high-wavenumber Raman peaks of this compound. More investigations should be carried out to ascertain the origin of this effect and, in particular, if it is related to the growth process or even to a photoinduced Eu^{3+} to Eu^{2+} valence change of the Eu ions. The latter, which has been previously reported for Eu_2O_3 fine particle films under 325-nm laser light irradiation,[26] could also explain the anomalous behavior of the Raman-active modes of this compound. In this context, we must also remind that RE sesquioxides are highly hygroscopic; a fact that could seriously affect their lattice dynamical properties, especially in powdered samples, thin films, and nanocrystals. More investigations should be thus carried out, in particular, by using single crystals like those used in the present work.

5 | CONCLUSIONS

We have reported a joint experimental and theoretical study of the lattice dynamics of C-type Tb_2O_3. Up to 16 Raman-active modes have been measured in a high-quality Tb_2O_3 single crystal. The comparison of experimental results with first-principles lattice dynamics calculations has allowed us to assign the symmetry of the experimentally observed Raman-active modes. We have shown that the zone-center Raman-active optical phonons of Tb_2O_3 follow the same trend as those of other RE and related sesquioxides with C-type or bixbyite structure. In this context, both our experimental RS measurements and our lattice dynamics calculations on Tb_2O_3, Dy_2O_3, Gd_2O_3, Eu_2O_3, and Sm_2O_3, which show a monotonic decrease of the Raman wavenumbers with increasing lattice parameter along the Tb_2O_3-Gd_2O_3-Eu_2O_3-Sm_2O_3-Dy_2O_3 series, prompt for a revision of the Raman spectra of Eu_2O_3 and also of some modes of Gd_2O_3. More investigations are required in order to

explain the anomalies reported in the literature for the high-wavenumber Raman-active modes of these two last compounds.

ORCID

Jordi Ibáñez http://orcid.org/0000-0002-8909-6541
Oriol Blázquez http://orcid.org/0000-0002-0921-2793
Sergi Hernández http://orcid.org/0000-0002-2226-1020
Plácida Rodríguez-Hernández http://orcid.org/0000-0002-4148-6516
Alfonso Muñoz http://orcid.org/0000-0003-3347-6518
Matias Velázquez http://orcid.org/0000-0002-8822-8207
Philippe Veber http://orcid.org/0000-0002-0204-1266
Francisco Javier Manjón http://orcid.org/0000-0002-3926-1705

REFERENCES

[1] T.-M. Pan, F.-H. Chen, J.-S. Jung, *J. Appl. Phys.* **2010**, *108*, 074501.

[2] C. H. Kao, K. C. Li, M. H. Lee, S. N. Cheng, C. H. Huang, W. K. Lin, *Thin Solid Films* **2012**, *520*, 3402.

[3] N. W. Gray, M. C. Prestgard, A. Tiwari, *Appl. Phys. Lett.* **2014**, *105*, 222903.

[4] I. Geppert, M. Eizenberg, N. A. Bojarczuk, L. F. Edge, M. Copel, S. Guha, *J. Appl. Phys.* **2010**, *108*, 024105.

[5] S. V. Belaya, V. V. Bakovets, A. I. Boronin, S. V. Koshcheev, M. N. Lobzareva, I. V. Korolkov, P. A. Stabnikov, *Inorg. Mater.* **2014**, *50*, 379.

[6] V. V. Bakovets, S. V. Belaya, M. N. Lobzareva, E. A. Maksimovskii, *Inorg. Mater.* **2014**, *50*, 576. (2014)

[7] P. Veber, M. Velázquez, G. Gadret, D. Rytz, M. Peltz, R. Decourt, *CrstEngComm* **2015**, *17*, 492.

[8] M. V. Abrashev, N. D. Todorov, J. Geshev, *J. Appl. Phys.* **2014**, *116*, 103508.

[9] K. A. Irshad, N. V. Chandra Shekar, T. R. Ravindran, V. Srihari, K. K. Pandey, *J. Mol. Struct.* **2017**, *325*, 1128.

[10] M. W. Urban, B. C. Cornilsen, *J. Phys. Chem. Solid* **1987**, *48*, 475.

[11] P. Hohenberg, W. Kohn, *Phys. Rev. B* **1964**, *36*, B864.

[12] G. Kresse, J. Furthmüller, *Comput. Mater. Sci.* **1996**, *6*, 15.

[13] P. E. Blöchl, *Phys. Rev. B* **1994**, *50*, 17953.

[14] G. Kresse, D. Joubert, *Phys. Rev. B* **1999**, *59*, 1758.

[15] J. P. Perdew, K. Burke, M. Ernzerhof, *Phys. Rev. Lett.* **1996**, *77*, 3865.

[16] J. P. Perdew, A. Ruzsinszky, G. I. Csonka, O. A. Vydrov, G. E. Scuseria, L. A. Constantin, X. Zhou, K. Burke, *Phys. Rev. Lett.* **2008**, *100*, 136406.

[17] H. J. Monkhorst, J. D. Pack, *Phys. Rev. B* **1976**, *13*, 5188.

[18] B. Garcia-Domene, H. M. Ortiz, O. Gomis, J. A. Sans, F. J. Manjón, A. Muñoz, P. Rodríguez-Hernández, S. N. Achary, D. Errandonea, D. Martınez-García, A. H. Romero, A. Singhal, A. K. Tyagi, *J. Appl. Phys.* **2012**, *112*, 123511.

[19] O. Gomis, D. Santamaría-Pérez, J. Ruiz-Fuertes, J. A. Sans, R. Vilaplana, H. M. Ortiz, B. García-Domene, F. J. Manjón, D. Errandonea, P. Rodríguez-Hernández, A. Muñoz, M. Mollar, *J. Appl. Phys.* **2014**, *116*, 133521.

[20] K. Parlinski, Phonon code, see http://www.computingformaterials.com/.

[21] N. D. Todorov, M. V. Abrashev, V. Marinova, M. Kadiyski, L. Dimowa, E. Faulques, *Phys. Rev. B* **2013**, *87*, 104301.

[22] W. B. White, V. G. Keramidas, *Spectrochim. Acta A* **1972**, *28*, 501.

[23] C. Kranert, R. Schmidt-Grund, M. Grundmann, *Phys. Stat. Sol. RRL* **2014**, *8*, 554.

[24] A. J. Silversmith, D. M. Boye, K. S. Brewer, C. E. Gillespie, Y. Lu, D. L. Campbell, *JOL* **2006**, *121*, 14.

[25] A. Ubaldini, M. M. Carnasciali, *J. Alloys Compd.* **2008**, *454*, 374.

[26] S. Mochizuki, F. Fujishiro, K. Ishiwata, *J. Phys. Conf. Ser.* **2005**, *21*, 189.

SUPPORTING INFORMATION

Additional supporting information may be found online in the Supporting Information section at the end of the article.